IOPscience iopscience.iop.org

Home Search Collections Journals About Contact us My IOPscience

Implantation-induced defects in $Hg_{0.78}Cd_{0.22}Te$ studied using slow positrons

This article has been downloaded from IOPscience. Please scroll down to see the full text article.

1995 J. Phys.: Condens. Matter 7 8529

(http://iopscience.iop.org/0953-8984/7/45/008)

View the table of contents for this issue, or go to the journal homepage for more

Download details:
IP Address: 171.66.16.151
The article was downloaded on 12/05/2010 at 22:25

Please note that terms and conditions apply.

J. Phys.: Condens. Matter 7 (1995) 8529–8538. Printed in the UK

Implantation-induced defects in $Hg_{0.78}Cd_{0.22}Te$ studied using slow positrons

L Liszkay†‡, C Corbel†, L Baroux†, P Hautojärvi§, A Declemy‖ and P O Renault‖

† INSTN-UEPEM CE Saclay, 91191 Gif-sur-Yvette Cédex, France

‡ KFKI Research Institute for Nuclear and Particle Physics, H-1525 Budapest 114, PO Box 49, Hungary

§ Laboratory of Physics, Helsinki University of Technology, 02150 Espoo, Finland

‖ Laboratoire de Métallurgie Physique, URA 131 CNRS, Avenue du Recteur Pineau, 86022 Poitiers Cédex, France

Received 6 July 1995

Abstract. Slow-positron-beam studies on aluminium-implanted mercury cadmium telluride are presented. Single crystals were implanted with 320 keV Al ions up to 3×10^{12} fluence at room temperature and 1×10^{14} ions cm^{-2} fluence at 100 K and 300 K. We discuss the effect of the native oxide layer on the positron spectra and show that the oxide–crystal interface acts as a strong positron trap. By using both the core (W) and the valence (S) annihilation fractions we can separate oxide-related positron effects at the surface from the damage in the crystal. Implantation introduces small vacancy clusters. On the basis of the relative Doppler parameters of the defects created ($S_d/S_b = 1.05$, $W_d/W_b = 0.80$), they are most probably divacancies. The divacancy profile is found to extend from the surface to a depth comparable to the mean Al implantation depth. At room temperature divacancy creation reaches saturation at 3×10^{12} ions cm^{-2} fluence with an estimated divacancy concentration of 4×10^{16} cm^{-3}. After implantation at low temperature (100 K) and annealing at 360 K the divacancy creation exceeds 10^{18} cm^{-3}.

1. Introduction

The $Hg_{1-x}Cd_xTe$ semiconductor (CMT) with a tunable bandgap is widely used in infrared sensor technology. Ion implantation is a standard technique used to achieve well controlled p–n junction structures in complex detector circuits with a large number of pixels. A well established property of ion implantation in CMT crystals is that an n^+ layer is created, independently of the ion species, indicating that the doping is induced by radiation damage [1]. There is, however, need of deeper knowledge on the microscopic structure of the defects created to control doping, optimize post-implantation processing and improve device quality.

Positron annihilation is a powerful technique for investigating vacancy-type defects in semiconductors. Its specific sensitivity for open-volume lattice defects has been widely used in studies of various compound semiconductors. In mercury cadmium telluride (MCT), negatively charged mercury vacancies (V_{Hg}^{2-}) have been directly identified using positrons in p-type annealed $Hg_{0.8}Cd_{0.2}Te$ single crystals [2–5] and epitaxial layers [6]. They have also been observed after electron irradiation in n-type converted crystals [7]. In addition, another vacancy signal, tentatively identified with the Te vacancy (V_{Te}), has been detected at low temperature in n^+-type electron-irradiated CMT [7].

0953-8984/95/458529+10$19.50 © 1995 IOP Publishing Ltd

In the present paper we report positron measurements on aluminium-implanted cadmium mercury telluride single crystals. To investigate the vacancy-type defects induced by ion implantation, we probe the samples by implanting low-energy positrons at various depths and measure the 511 keV annihilation lineshape as a function of the positron energy. In the first part of the paper we analyse the positron spectra of the unimplanted substrate material and demonstrate the effect of a native oxide layer formed after long storage in air. In the second part we investigate defects in implanted HgCdTe. We show that the defects which trap positrons have the characteristics of vacancy clusters.

2. Experimental details

The $Hg_{0.78}Cd_{0.22}Te$ substrate was grown in the Société Anonyme de Télécommunication (SAT) using the travelling heater method (THM). After stoichiometric annealing, Hall effect measurements showed that the crystals had n-type conductivity with a charge carrier concentration of 2 to 6 $\times$ 10^{15} cm^{-3} at 77 K. Ion implantation was performed at room temperature with 320 keV aluminium ions up to doses 3 $\times$ 10^{12} and 1 $\times$ 10^{14} cm^{-2}. A third crystal was implanted with up to 1 $\times$ 10^{14} cm^{-2} at 100 K and subsequently annealed at 360 K in air.

We used a high-purity germanium detector to measure the Doppler broadening of the 511 keV annihilation lineshape as a function of the positron energy. The beam energy E was varied in 0.5 keV steps between 0.5 keV and 25 keV. At each energy value, more than 10^6 events were collected into the annihilation peak by a digitally stabilized multichannel analyser. The lineshape of the annihilation peak was described by two conventional Doppler parameters S and W.

The S or valence annihilation parameter was defined as the relative fraction of the annihilation events in the γ energy range where $|E_\gamma - 511\ \mathrm{keV}| < 0.83$ keV. This range corresponds to electron–positron annihilations with a centre-of-mass momentum $p < 3.3 \times 10^{-3} m_0 c$ (where m_0 is the electron mass and c is the velocity of light in vacuum), arising mainly from valence electrons of the crystal. The W or core annihilation parameter was defined with $2.49\ \mathrm{keV} < |E_\gamma - 511\ \mathrm{keV}| < 7.30$ keV energy windows. This energy range corresponds to annihilation events with $10 \times 10^{-3} m_0 c < p < 29 \times 10^{-3} m_0 c$ momentum, arising only from core electrons.

Positron annihilation at a vacancy-type defect gives rise to annihilation parameters (W_d, S_d) different from those in the lattice (W_b, S_b). They can be used as the fingerprint of the defect. The larger the open volume, the lower the core annihilation fraction W_d and the higher the valence annihilation fraction S_d. If the experimental annihilation lines (W, S) are superpositions of two characteristic lines, e.g. one corresponding to the crystal bulk and the other to a defect d, then

$$(S, W) = (1 - f_d)(S_b, W_b) + f_d(S_d, W_d) \tag{1}$$

where f_d is the annihilation fraction in the defect d. Consequently, when f_d varies, the experimental lineshape parameters fall on a straight line in the (W, S) plot [8]. The slope of this line

$$R_d = \left| \frac{S - S_b}{W - W_b} \right| \tag{2}$$

is also a defect-characteristic parameter. It is independent of the annihilation fraction f_d and thus of the defect concentration. It can be deduced from the experimental data by linear regression even if the defect parameters S_d and W_d are not known. In the present paper,

we use the normalized parameter $R_d^* = R_d(W_b/S_b)$ which is less dependent than R_d on the experimental energy windows used to define S and W.

The fraction of positrons annihilating at different depths is determined by the positron stopping profile and by the subsequent thermal diffusion and trapping [9]. We analysed the experimental $S(E)$ and $W(E)$ curves by means of the VEPFIT program [10]. We introduced minor changes into the code to allow simultaneous fits of both $S(E)$ and $W(E)$ curves in one step. In the analysis, the positron stopping profile in HgCdTe was given by the Makhovian distribution as [11]

$$P(z) = \left(\frac{1.8}{z_0}\right)\left(\frac{z}{z_0}\right)^{0.8} \exp\left[-\left(\frac{z}{z_0}\right)^{1.8}\right] \tag{3}$$

where $z_0 = 1.13\bar{z}$ and $\bar{z}$ is the mean penetration depth given by $\bar{z} = 5.46 \times E^{1.6}$ ($\bar{z}$ is measured in nm, E in keV).

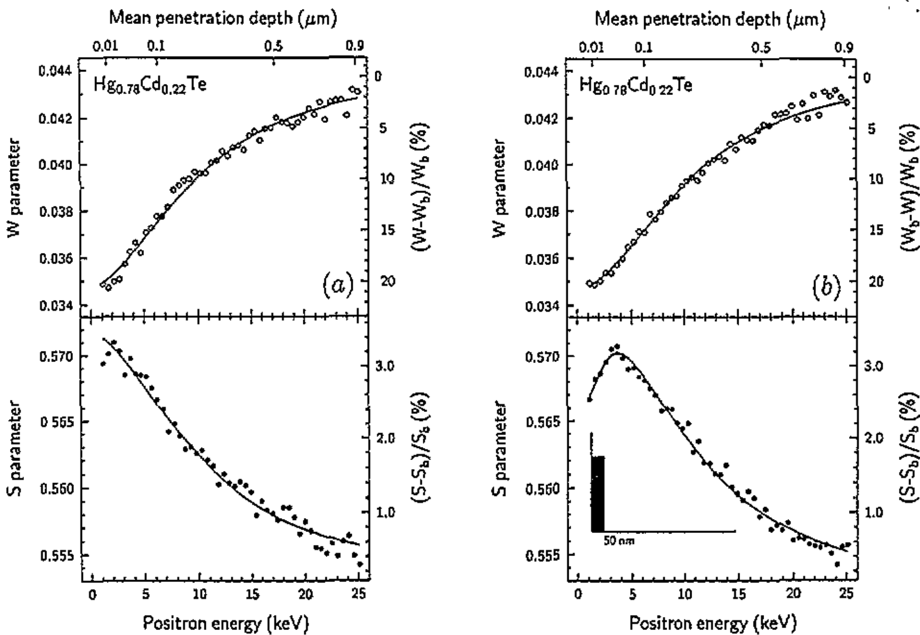

Figure 1. Valence (S) and core (W) annihilation fractions as a function of the positron beam energy in $Hg_{0.78}Cd_{0.22}Te$ single crystals. (a) Freshly etched crystal. (b) After storage in air. The continuous line represents the result of the simultaneous fits of both S and W parameters.

3. Results

Figure 1 demonstrates how the energy dependence of the S and W annihilation fractions in unimplanted CMT samples are affected by long storage in air. In an n-type crystal, freshly etched in Br–methanol solution (figure 1(a)) the valence annihilation fraction $S(E)$ decreases continuously from 0.571 to 0.555 with increasing positron energy. The W parameter varies in an opposite way, like the mirror image of S. Figure 1(b) shows that when, after etching, the crystal is stored (aged) for several months in air at room temperature, the $S(E)$ curve goes through a maximum at about 3.5 keV beam energy, while the $W(E)$ curve is practically identical in the as-etched and aged crystals.

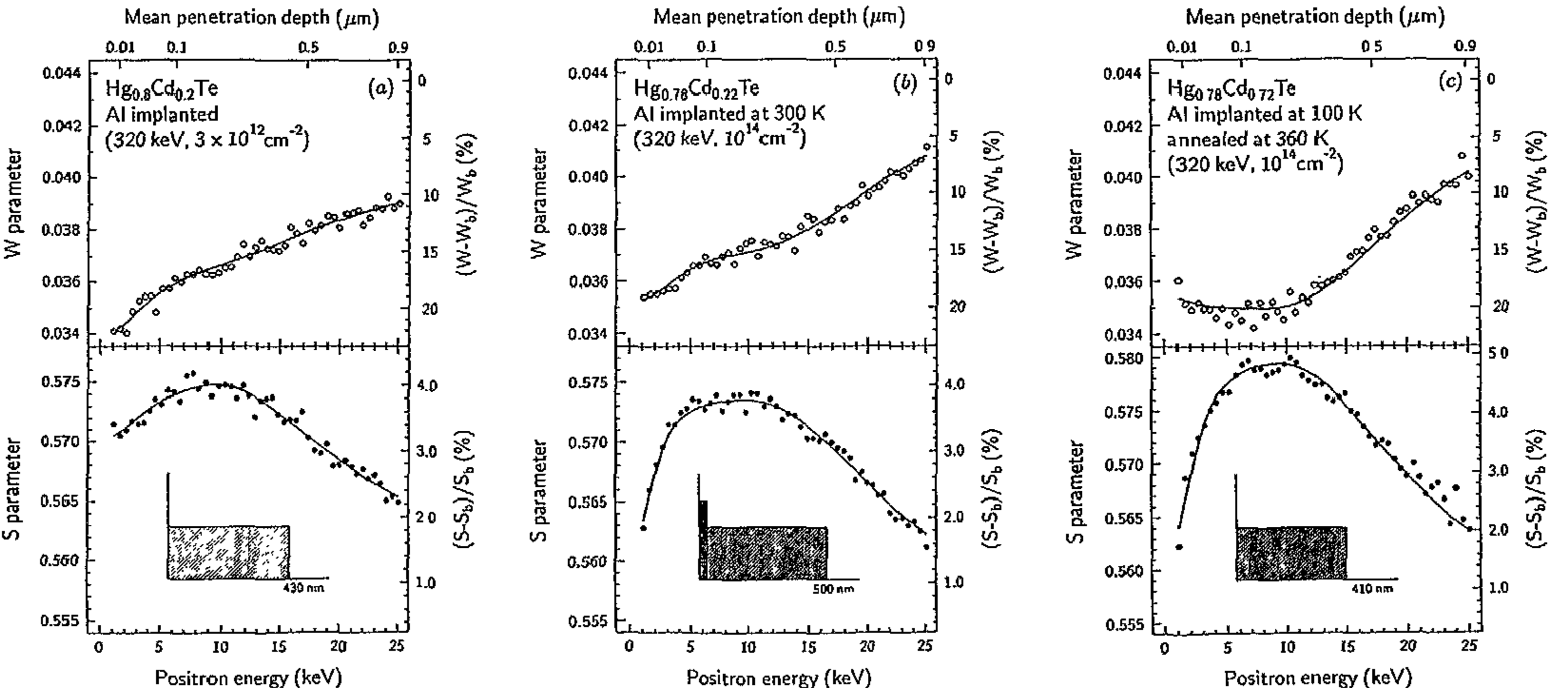

Figure 2. Positron annihilation Doppler parameters as a function of the positron energy in aluminium-implanted $Hg_{0.78}Gd_{0.22}Te$ samples. Implantation was performed with 320 keV ions at room temperature to: (a) 3×10^{12} cm^{-2} fluence; (b) 1×10^{14} cm^{-2} fluence; (c) 1×10^{14} cm^{-2} fluence at 100 K, and subsequently annealed at 360 K in air. At the bottom of each curve the schematic representation of the fitted divacancy profile is displayed (the corresponding fitted curves are drawn with solid lines).

Implantation with aluminium ions has a huge effect on positron behaviour as seen in figure 2. In all samples, the $S(E)$ curve has a broad maximum at around $E = 5$–10 keV. At higher positron energies, $S(E)$ decreases and approaches the S value we found in the unimplanted substrate. It is noticeable that the maximum of the S parameter (S_{max}) is around 0.574 both at 3×10^{12} (figure 2(a)) and 1×10^{14} cm² (figure 2(b)) aluminium ion fluences at room temperature. This is well above the asymptotic S value found in the unimplanted CMT crystal. After implantation at 100 K with a 1×10^{14} cm^{-2} dose and annealing at 360 K, S_{max} increases to 0.579. In contrast with the energy dependence of the valence annihilation fraction S, there is no broad plateau in $W(E)$ in any of the samples implanted at room temperature, although a small bulge is seen in the 7–13 keV range at the higher implantation fluence. The core annihilation fraction W increases over all of the energy range studied in these spectra. After low-temperature implantation both $S(E)$ and $W(E)$ had a broad extremum between 1.5 and 11 keV.

The last point worth mentioning concerns the correspondence between variations of $S(E)$ and $W(E)$. As we have seen in the case of the substrate that was stored for a longer time in air, in some cases there is no negative correlation between the two curves. We noticed that in the low-energy part of some spectra (0–5 keV in figure 1(b), 0–10 keV in figure 2(a), 0–5 keV in figure 2(b)) S and W vary in the same direction while elsewhere they are anticorrelated. It is always at lower energies, i.e. near the surface, that the two Doppler parameters increase or decrease together as a function of the positron energy. Since S and W are generally anticorrelated in different annihilation states of the same material (a defect with a higher S than another shows a lower W), parallel changes at low positron energies imply the existence of an overlayer on the surface with a different chemical composition to that of the semiconductor crystal.

4. Discussion

4.1. Oxide layer on unimplanted CMT

Comparison of the $S(E)$ curves after etching (figure 1(a)) and after long storage in air (figure 1(b)) shows that a thin layer near the sample surface was modified by the storage. Immediately after etching S and W parameters vary smoothly from the surface values (S_s, W_s) to the values in the crystal continuum (S_c, W_c). To check whether positron annihilation can indeed be described as the superposition of two annihilation states, we plot the beam-energy-dependent $S(E)$ values as a function of $W(E)$ in figure 3(a). This reveals that the relation between S and W is indeed linear. The linearity of the S versus W curve suggests that in the as-etched sample there are only two distinct sites where annihilation takes place [8]: the sample surface (S_s, W_s) and the interior of the crystal (S_c, W_c). When the beam energy increases, the probability $f_s(E)$ that positrons annihilate on the surface decreases and the annihilation parameters (S, W) tend towards the values (S_c, W_c) in the crystal. The curves $S(E)$ and $W(E)$ can be fitted simultaneously to the expressions $S(E) = f_s(E)S_s + (1 - f_s(E))S_c$ and $W(E) = f_s(E)W_s + (1 - f_s(E))W_c$ where the probability $f_s(E)$ that positrons annihilate on the surface is calculated by taking into account the positron stopping profile (equation (3)) and diffusion. We obtained the best fit for the annihilation parameters $S_c = 0.5526 \pm 0.0003$ and $W_c = 0.04373 \pm 0.0005$, and for the positron diffusion length $L^+ = 250 \pm 20$ nm. We found the same values for (S_c, W_c) in other stoichiometric annealed $Hg_{0.8}Cd_{0.2}Te$ crystals as well. These values are the lowest S_c and the highest W_c we have measured in CMT crystals with similar composition. For this reason, we conclude that they characterize the annihilation of free positrons in the lattice, i.e.

$S_b = S_c$ and $W_b = W_c$. The estimated diffusion coefficient $D^+ = L^2/\tau = 2.2 \pm 0.5$ cm^2 s^{-1} is close to those of free positrons in other compound semiconductors [11]. The relatively large uncertainty of the determination of positron diffusion length can be explained by annihilation in a few-nanometre-thick overlayer.

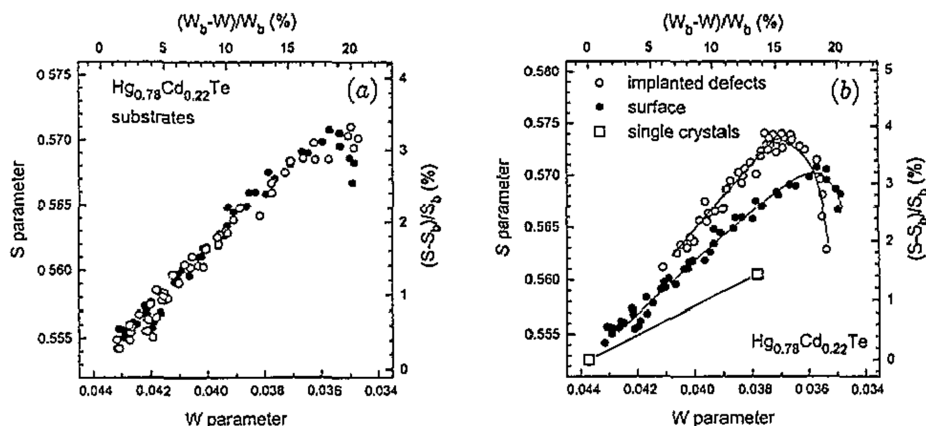

Figure 3. Valence annihilation fraction S as a function of the core annihilation fraction W. (a) $Hg_{0.78}Cd_{0.22}Te$ substrates: (●) freshly etched crystal; (○) after storage in air. The overlap between the two curves shows that both the surface (●) or thin layer/crystal interface (○, see the text) and the crystal have the same positron annihilation properties. (b) As-etched and implanted $Hg_{0.78}Cd_{0.22}Te$. For comparison, the Doppler parameters of a crystal showing saturated positron trapping in mercury monovacancies are given. Fitted curves are displayed as continuous lines. The slope of the linear part of the curves defines the R parameter of the different positron traps: implantation-induced defect, oxide–crystal interface and mercury vacancy.

For the sample stored in air after etching, the (S, W) data lie on a straight line only above 3.5 keV (figure 3(a)). It follows that the positrons implanted with energy higher than 3.5 keV are shared between two annihilation states whereas at lower energies of 0–3.5 keV a third annihilation site becomes dominant. To understand what happens in this region, we examine figures 1(a) and 1(b) in more detail. We note that the Doppler S parameter has the same value ($S = 0.571$) at $E \approx 0$ keV in the etched sample and at the maximum of the S curve of the aged sample in figure 1(b). The corresponding W values are nearly equal as well. Moreover, the $(W(E), S(E))$ data points lie on the same line above the energy corresponding to the maximum of the S curve. This leads us to the conclusion that the same annihilation site is responsible for both the surface signal S_c in the freshly etched sample and for the maximum at 3.5 keV after long storage in air.

The observed effects at low positron energy are connected to changes in the near-surface layer of the sample. The positron results show that the overlayer has the following properties: (i) it is formed immediately after etching and (ii) it grows thicker after long storage in air. A possible explanation is that it is a thin defect layer near the sample surface. It may thicken due to mercury outdiffusion [12]. As is shown in figure 3(b), superposition of annihilation signals from the crystal lattice and the surface or interface annihilation site gives a slope which is remarkably different from the ones obtained when the superposition of annihilation in mercury monovacancy V_{Hg} or the implantation-induced defect and the crystal lattice are measured. The relative S parameter, $S/S_b = 1.035 \pm 0.001$, is much higher than that of the mercury monovacancy (where $S/S_b = 1.015 \pm 0.001$ according to [13]) and the R^* parameter of the surface/interface is significantly different from the value

found for either the monovacancy V_{Hg} or the implantation-induced defect (table 1). These values would suggest the formation of vacancy clusters near the surface. Nevertheless, as we have seen above, the observed correlation between the S and W annihilation fractions at low positron energy can be better explained by a near-surface layer with a chemical composition different from that of the substrate material.

Another process which modifies the surface is oxidation. The freshly etched CMT surface is prone to forming a thin oxide layer, rich in TeO_2 [14]. The oxide layer is thin in the freshly etched sample but becomes thicker after longer storage in air. The imperfect structure of the native oxide layer is likely to contain a high concentration of positron traps. After implantation of positrons into the crystal interior a fraction of them start to diffuse back towards the surface. Back-diffusing positrons meet the oxide/crystal interface which acts as an effective trap for them. The annihilations at the interface produce the 'surface' parameter S_c seen at about $E = 1$–2 keV in the freshly etched sample and a deeper one at $E = 3.5$ keV after long storage in air. In the second case, positrons implanted at $E < 3.5$ keV are stopped in the oxide layer and have possible annihilation states in the layer, at the vacuum/oxide surface and oxide/crystal interface. We can attribute the near-surface positron effect to positron trapping at the oxide/crystal interface. The freshly etched sample has a very thin oxide layer: at 1 keV positron energy most of the positrons are already implanted behind the oxide and, due to the subsequent back-diffusion, annihilate at the strongly trapping surface.

The thickness of the oxide layer on the oxidized crystal can be easily estimated from the mean positron implantation depth at the maximum of the S curve in figure 1(b) as being approximately 30 nm. A quantitative analysis of the experimental data is made describing the oxide/crystal interface as a totally absorbing layer for diffusing positrons. The positron characteristics of the interface are fixed to the surface values of the as-etched layer. If the positron diffusion length in the oxide is of the order of the layer thickness or greater and both the surface and the interface are total absorbers for positrons, then all positrons annihilate either at the vacuum/oxide surface or at the oxide/crystal interface. From figure 1(b) we find $S_s = 0.5650$ and $W_z = 0.0345$ as surface values. Using the density of TeO_2 as the density of the oxide overlayer, a thickness of 50 ± 5 nm for the oxide layer gives the best fit for the experimental $S(E)$ and $W(E)$ curves.

4.2. *Vacancy clusters in implanted CMT*

The broad maximum with a high S value in all implanted samples shows that vacancy-type lattice defects are created by 320 keV aluminium ions. Despite the difference of almost two orders of magnitude between the implantation fluences (3×10^{12} and 1×10^{14} cm^{-2}) comparison of figures 2(a) and (b) reveals that the maximum of the S parameter is the same in the two samples. Consequently, either the positron trapping or the concentration of defects created by ion implantation has already reached its saturation level at the lower, 3×10^{12} Al cm^{-2} fluence. In the first alternative, the defect concentration is so high that all positrons annihilate trapped. We, however, prefer the second alternative: above a critical implantation fluence the defect concentration ceases to increase. This second alternative seems more likely for the following reasons: saturation in sheet carrier concentration has been found in mercury cadmium telluride after implantation with light boron ions at around 10^{13} ions cm^{-2} fluence [1]. In the case of argon ions, the sheet electron concentration is already saturated at above 10^{12} ions cm^{-2} dose [15]. Although the sensitivity of the methods applied (transmission electron microscopy, channelling) was not sufficient to indicate the presence of lattice defects at this dose, the saturation effect is certainly connected with

lattice defects created by the implantation. In the present case the higher implantation energy (320 keV instead of 150 keV of both [1] and [15]) and ion mass higher than that of the boron may well lead to saturation both in carrier concentration and the production of positron traps even at 3×10^{12} ions cm^{-2} fluence.

We applied a simple defect profile model in order to find out the depth distribution of the damage created in the three implanted crystals. We took a block profile with a constant defect concentration (i.e. constant S and W) up to a cut-off depth beyond which the crystal was undefected. The Doppler parameters of the surface and the defected region (S_{damage}, E_{damage}) as well as the depth of the profile were fitted. In addition, on the basis of the positron diffusion length in the damaged region, the fitting gives a rough estimate for the (S_d, W_d) parameters of the defects created. In the case of the sample with the 1×10^{14} cm^{-2} fluence (figure 2(b)) a 30 nm thin oxide layer, with properties as discussed above, had to be introduced at the sample surface to get consistent results for both $S(E)$ and $W(E)$ curves simultaneously. The $S(E)$ curve alone could be fitted without the oxide layer with almost the same results but the resulting model was not consistent with $W(E)$.

The results are given in table 1. The solid lines in figures 2 and 3(b) are the fitted curves. As we expected, the two samples implanted at 300 K have nearly the same Doppler parameter in the damaged region. The depth of the defect profile at lower fluence (420 nm) is slightly less than that at high fluence 500 nm). The Doppler parameters are $S_{damage} = 0.5761 \pm 0.0005$ and $W_{damage} = 0.0371 \pm 0.0002$, corresponding to $S_{damage}/S_b = 1.042 \pm 0.002$ and $W_{damage}/W_b = 0.847 \pm 0.003$. In addition to the S_{damage}, W_{damage} annihilation fractions, which are superpositions of annihilation signals from both the lattice and the defects created by implantation, the defect-specific parameters S_d and W_d can be estimated on the basis of the effective positron diffusion length in the damaged region. Fitting of the S parameter of the defect created yielded $S_d = 0.5800 \pm 0.001$ for the defect parameter (corresponding to $S_d/S_b = 1.050 \pm 0.002$) in the case of the lower implantation dose. The oxidized surface of the other crystal made the application of the defect parameter analysis impossible. Nevertheless, one can use a model with positron trapping in defects with the same S_d and obtain good agreement with the experimental data.

After implantation at 100 K and annealing at 360 K we found different Doppler parameters of the damaged region. S_{damage} increased to 0.5800 ± 0.0004 and W_{damage} decreased to 0.0349 ± 0.0001, giving a relative S_{damage}/S_b ratio of 1.050 ± 0.001 and $W/W_b = 0.80 \pm 0.002$. Since the defect parameter R^* is nearly equal after irradiation at room temperature ($R^* = 0.27 \pm 0.01$) and at 100 K ($R^* = 0.25 \pm 0.01$), we can conclude that the same defect is responsible for the positron trapping in all implanted crystals. The wide plateaus in both $S(E)$ and $W(E)$ curves (figure 2(c)) and the sharp increase of S at low energy strongly suggest that the positron trapping in the damaged region is in saturation and thus $S_d = S_{damage}$. We find then that the S_d defect parameter is the same as the S_d determined for the room temperature implanted samples. This observation confirms that the observed saturation effect at room temperature is the result of saturation in defect creation. In summary, on the basis of both the R^* and S_d/S_b defect parameters we can thus conclude that the same type of defect traps positrons in all implanted samples. This defect has comparable concentration after aluminium implantation with 3×10^{12} and 1×10^{14} ions cm^{-2} fluence at room temperature. Low-temperature implantation results in a higher defect concentration which saturates positron trapping.

Previous studies reported 1.017 [5] and 1.020 [16] as relative S_v/S_b parameters for the mercury monovacancy in $Hg_{0.8}Cd_{0.2}Te$ single crystals. In p-type annealed samples where positron trapping at V_{Hg} was saturated according to positron lifetime studies, $S_v/S_b = 1.015$ and $W_v/W_b = 0.865$ were measured [13]. The higher S_d/S_b ratio we find here for

implantation-induced defects suggests that the positron traps created by implantation are larger than a monovacancy. The defect-specific R^* parameter, which is 0.11 ± 0.02 in the case of the mercury monovacancy and 0.26 ± 0.02 in the implanted defects shows clearly that the defect type is different in the two cases (table 1).

Table 1. Relative S_{damage} and W_{damage} values, the depth d of the fitted defect profile and the $R^* = (\Delta S/\Delta W)(W_b/S_b)$ defect-specific positron parameter in the damaged region of Al-implanted CMT samples and at the crystal/oxide interface. For comparison, parameters for the mercury monovacancy are given as well.

Sample/dose	S/S_b	W/W_b	d (nm)	R^*
3×10^{12} cm^{-2}	1.042(2)	0.847(3)	430(10)	0.278
1×10^{14} cm^{-2}	1.038(2)	0.853(3)	500(10)	0.261
1×10^{14} cm^{-2} (100 K)	1.050(2)	0.800(3)	410(10)	0.247
CMT–oxide interface	1.035	0.805		0.179
Implanted defect	1.05	0.80		0.26
Hg monovacancy†	1.015	0.865		0.111

†From [13].

As we demonstrated earlier [8], the experimentally determined relative W parameter (W_d/W_b) can be compared with the ratio between calculated core annihilation fractions (A/A_b) in order to identify the positron traps. The theoretical estimate for the relative core annihilation fraction of the A/A_b is 0.910 for the V_{Hg} and 0.810 for the V_{Hg}–V_{Te} divacancy [17]. We can therefore expect that the difference between the W_d/W_b values of the two defects is approximately 0.10. We found that the characteristic relative core annihilation parameter for the mercury vacancy ($W/W_b = 0.865$) is 0.08 higher than that of the defect found in the implanted region ($W/W_b = 0.799$). The difference is thus smaller than the expected difference between monovacancy and divacancy. Although the theoretical estimate does not take into account lattice relaxation and some other possible effects and therefore must be handled with due caution when comparing with the measured data, the comparison shows that the prevailing positron trapping defect type in the implanted zone is most probably not larger than a divacancy.

We can estimate the concentration of the created defects after implantation at room temperature from the Doppler parameters of the defected zone. The trapping rate of positrons in this region is

$$\kappa = \frac{S_d - S}{S - S_b}\lambda_b = 0.9 \pm 0.6 \text{ ns}^{-1} \tag{4}$$

where S is the Doppler parameter in the damaged zone. If we take $\mu = 10^{15}$ atom s^{-1} as typical positron trapping coefficient in semiconductors at 300 K [18], the defect concentration can be calculated as $c_d = \kappa/\mu = 1 \times 10^{-6}$/atom $= 4 \times 10^{16}$ cm^{-3}. In the case of the sample implanted at 100 K the positron trapping is at saturation and the above calculation is not possible. On the basis of the saturated trapping, we can estimate that the defect concentration is higher than 10^{18} cm^{-3}.

The depth of the implantation-induced damage as determined by the analysis of the positron spectra is 400–500 nm in all samples (table 1). This value corresponds well to the width of the stopping profile of the aluminium ions, which is approximately 400 nm. Hence, the positron annihilation result supports earlier investigations which found that in the case of light ions the damaged region is near the penetration depth of the implanted ions [1].

5. Conclusions

We found that aluminium implantation creates a high concentration of positron trapping defects within the stopping range of the ions. The damaged region contains small vacancy clusters, most likely divacancies. Saturation in the divacancy creation occurs at room temperature as low as 3×10^{12} ions cm^{-2} fluence. Implantation at 100 K creates higher concentration of the divacancies causing saturation in positron trapping. The divacancy concentration, estimated from the positron trapping is of the order of 10^{16} cm^{-3} after implantation at 300 K and more than 10^{18} cm^{-3} at 100 K.

Acknowledgments

We are grateful to the Société Anonyme de Télécommunication (SAT) for providing the substrate material. One of the authors (LL) has received partial support from the National Scientific Research Fund (OTKA grant No 1833). Travel support from the Soros Foundation, the Roland Eötvös Physical Society and the OMFB-CIMO (Hungarian-Finnish grant No 13) is gratefully acknowledged.

References

[1] Destéfanis G L 1988 *J. Cryst. Growth* **86** 700
[2] He Y J, Li X F, Li L G, Yu W Z and Xiao J R 1989 *J. Phys.: Condens. Matter* **1** SA91
[3] Krause R, Klimakow A, Kiessling F M, Polity A, Gille P and Schenk M 1990 *J. Cryst. Growth* **101** 512
[4] Gély C, Corbel C and Triboulet R 1992 *J. Phys.: Condens. Matter* 2 4763
[5] Smith C, Rice-Evans P C, Shaw N and Smith D L 1992 *J. Phys.: Condens. Matter* **4** 5825
[6] Smith C, Rice-Evans P C, Shaw N and Smith D L 1993 *Phil. Mag. Lett.* **67** 213
[7] Kiessling F *et al* 1995 to be published
[8] Liszkay L, Corbel C, Baroux L, Hautojärvi P, Bayhan M, Brinkman A W and Tatarenko S 1994 *Appl. Phys. Lett.* **64** 1380
[9] Schultz P J and Lynn K G 1988 *Rev. Mod. Phys.* **60** 701
[10] van Veen A, Schut H, de Vries J, Hakvoort R A and Ijpma M R 1990 *Positron Beams for Solids and Surfaces (AIP Conference Proceedings 218)* ed P J Schultz, G R Massoumi and P J Simpson (New York: American Institute of Physics) p 171
[11] Soininen E, Mäkinen J, Beyer D and Hautojärvi P 1992 *Phys. Rev.* B **46** 13 104
[12] Neubert M, Kiessling F M, Barz B and Jacobs K 1993 *J. Cryst. Growth* **128** 604
[13] Baroux L *et al* unpublished
[14] Kowalczyk S P and Cheung J T 1981 *J. Vac. Sci. Technol.* **18** 944
[15] Shastov K V 1992 *Phys. Status Solidi* a **130** 293
[16] Smith C D, Rice-Evans P C and Shaw N 1994 *Phys. Rev. Lett.* **72** 1108
[17] Plazaola F, Seitsonen A P and Puska M J 1994 *J. Phys.: Condens. Matter* **6** 8809
[18] Hautojärvi P 1995 *Mater. Sci. Forum* **175–8** 47